

Please cite as:

R. Natu, M. Islam, R. Martinez-Duarte “[Nondimensional Streaming Dielectrophoresis Number for a System of Continuous Particle Separation](#)” *Analytical Chemistry*, 91 (7), 4357-4367 (2019).

Non-dimensional Streaming Dielectrophoresis Number for a System of Continuous Particle Separation

Rucha Natu, Monsur Islam and Rodrigo Martinez-Duarte

Multiscale Manufacturing Laboratory, Department of Mechanical Engineering, Clemson University, SC USA
29634

ABSTRACT: Cell sorting methods are required in numerous healthcare assays. Although flow cytometry and magnetically actuated sorting are widespread techniques for cell sorting, there is intense research on label-free techniques to reduce the cost and complexity of the process. Among label-free techniques, Dielectrophoresis (DEP) offers the capability to separate cells not only based on size but also on their membrane capacitance. This is important because it enables cell discrimination based on specific traits such as viability, identity, fate and age. StreamingDEP refers to the continuous sorting of cells thanks to the generation of streams of targeted particles by equilibrating the drag and DEP forces acting on targeted particles. In this work, we provide an analytical expression for a StreamingDEP number towards enabling the *a priori* design of DEP devices to agglomerate targeted particles into streams. The non-dimensional StreamingDEP Number (SDN) obtained in this analysis is applied to experiments with 1 μm polystyrene particles and *Candida* cells. Based on these experiments, three characteristic zones are mapped to different values of the SDN: 1) physical capture thanks to DEP for $0 < \text{SDN} < 0.6$; 2) streaming due to DEP for $0.6 < \text{SDN} < 1$; and 3) elution without experiencing DEP for $\text{SDN} > 1$.

1. Introduction

Cell sorting is the cornerstone for many healthcare assays. Although flow cytometry [1–3] and magnetically actuated cell sorting [4,5] are widespread techniques used for continuous and high throughput cell sorting, the use of fluorescent and magnetic labels drastically increase the cost and time of the process due to required incubation of the cell sample with often expensive labels. Moreover, the effect of labels on the therapeutic use of sorted cells is still unclear [6]. Hence, intensive research is on label-free techniques to sort cells out of a culture, such as deterministic lateral displacement (DLD) [7,8], inertial microfluidics [9,10], and acoustophoresis [11,12]. These high throughput techniques mostly utilize the variation in size and shape of the targeted cells to discriminate them from their background but face limitations since using size and shape as markers lacks specificity. Dielectrophoresis (DEP) is an alternative to these techniques since it is also a label-free technique but can enable higher specificity by exploiting both cell size and membrane capacitance to discriminate targeted cells from their background. DEP refers to the motion of an induced electrical

dipole when under the action of an electric field gradient. Hence, exposing an electrically neutral but polarizable cell to an electric field gradient causes it to polarize and interact with the field. Depending on the electrical polarizability of the cell compared to its suspending media at any given field frequency, the cell can either move towards the field gradient, as in positiveDEP, or away from it as in the case of negativeDEP. PositiveDEP is seen when the cell is more polar than the media [13]. Of note, different techniques exist to implement the required field gradient for DEP and can be largely classified as electrode-based DEP (eDEP) or insulator-based DEP (iDEP) [14]. Insulator-based DEP relies on arrays of insulating structures to distort an otherwise uniform electric field implemented using parallel electrodes. At field frequencies from kHz to MHz, the electrical polarizability of the cell depends on its size and membrane capacitance; which affords for high specificity. For example, membrane capacitance has been used as a marker to detect early apoptosis [15,16], and track circadian rhythms [17]. Membrane capacitance is also known to change due to cell viability, age, identity and fate [18,19].

Up to date, DEP is mostly used as a batch sorting technique where cells are isolated from a sample by trapping them in specific locations using positive DEP and then released at different times. The caveats of this approach are that particles are exposed to the electric field for long periods of time, which can impact their viability [20], and that throughput is usually low since the DEP force must overcome the drag force on the particle to achieve trapping. To overcome these limitations, continuous sorting has traditionally been done using negative DEP, in a technique also known as focusing, where cells or particles flowing through a channel are *repelled* from electric field gradients positioned in strategic locations to push targeted cells or particles into forming streams [21-24]. Since the magnitude of repulsion depends on the cell or particle's properties, one can specify the distance of the stream from the field gradient. Alternatively, one can generate streams of cells or particles by selectively *attracting* them to the field gradient in a technique called streaming DEP. The use of streaming DEP is important because it opens a whole region of the device that is underutilized when limited to focusing with negative DEP only. In streaming DEP, the targeted particles or cells flowing in the device are *attracted* to the field gradient using positive DEP, but instead of trapping they are carried away in characteristic flow lines, hence forming streams as it is shown in this present work. Streaming DEP as describe in this work only occurs when an equilibrium exists between positive DEP and other forces such as drag acting on the targeted cell or particle.

Only few authors have reported continuous particle sorting using streaming DEP. Cummings et al. introduced the concept by demonstrating the agglomeration of 200 nm-diameter latex particles into characteristic streams around regions of high electric field gradient [25,26]. The Ros group then exploited the benefits of streaming DEP for the continuous separation of biomolecules [25-29]. For example, Nakano et al. reported streaming DEP of proteins Immunoglobulin G and bovine serum albumin using insulator-based DEP in combination with electroosmotic flow [27]. Recently, we reported the computational modeling of streaming DEP for stem cells using an electrode array [30], where the use of cylindrical electrodes was determined to be beneficial over other square and diamond electrode geometries.

The contribution of the present work is providing an analytical expression to predict the experimental conditions that result in streaming DEP of a targeted particle or cell. To this end, we first show experimental images of streaming DEP behavior in cells and particles to support and serve as background for the derivation of an expression for a streaming DEP number (SDN); which depends on flow velocity in the channel, voltage and frequency of the polarizing signal, cell electrical properties and dimensions of an array of cylindrical electrodes. We then assess the use of the SDN to evaluate the streaming DEP behavior of latex particles and *Candida* cells. Lastly, we discuss the implications of these results on the continuous separation of cells of interest using streaming DEP.

2. Background and Theory

2.1 The concept of streaming DEP

Preliminary experiments showed the streaming DEP behavior of *Candida* cells and latex particles as illustrated in figure 1A and B respectively. Streams of cells and 1 μm -diameter particles can be observed in both figures as the lines that are co-linear with the regions of high electric field located around the cylindrical carbon electrodes in this case. Streaming DEP is possible due to the equilibrium between the DEP and drag forces acting on the cells or particles. Such force interaction can lead to three different scenarios: 1) trapping, 2) streaming thanks to positive DEP, or 3) elution without any DEP influence. If DEP overcomes drag, the cell or particle will be trapped on the carbon electrodes as extensively reported elsewhere [31-35]; if drag overcomes DEP the particle is eluted away without any influence from the DEP force and any sorting is solely due to cell size or shape.

Figure 1B further shows how streaming DEP can be used in tandem with traditional focusing using negative DEP. Latex particles of different diameters, 1 and 10 μm , could be separated into two different streams: 1 μm -diameter particles stream due to streaming DEP while 10 μm -diameter particles focus in between the electrodes due to negative DEP.

Based on these preliminary results, we aimed at deriving a streaming DEP number, or SDN, as a non-dimensional quantity that reflects the interconnection between different system parameters and allows for the prediction of streaming behavior for a particle that enters the channel at a given X_{in} . This is important because it can provide guidelines in the design of the DEP device, such as size and geometry of the electrode array; and of the experimental parameters, i.e. flow velocity, polarizing

signal, to achieve streaming of a targeted cell or particle.

2.2 Definition of variables, region of analysis (ROA), and assumptions

StreamingDEP can be implemented using electrodes or insulating structures. Although this work will emphasize the use of electrodes to generate a field gradient, this analysis is expected to also apply to insulator-based DEP. For the sake of simplicity, here we use the term particle to refer to cells and particles. Based on our previous work on comparing different electrode cross-sections for streamingDEP [30], we focus on the study of electrodes with cylindrical cross-section. We assume a pressure-gradient in the channel and a parabolic flow profile. The experimental device features an array of N columns and M rows of cylindrical electrodes with radius r_e and polarized by a voltage V . The array is contained in

a microfluidic channel, of width w , with the direction of the flow assumed from left to right (figure 1C). All electrodes in the array are assumed to be as tall as the channel height H , hence obstructing the flow in the channel. The center-to-center distance between electrodes can be different between columns and rows and is denoted by C_x in the X axis (rows) and C_y in the Y axis (columns). The Z axis is along the height of the channel H . Since a minimum number of columns are expected to be necessary to focus particles into streams in the channel, the importance of columns supersedes that of rows in streamingDEP. Hence, we simplify our analysis to the central row of electrodes in the array first and then to one-half of such a row due to symmetry to obtain the ROA shown in fig. 1C inset located in a given X-Y plane located at a specific height h along the total height H of the channel. Of note, the effect of the channel walls on particle behavior is expected to be underestimated in this ROA.

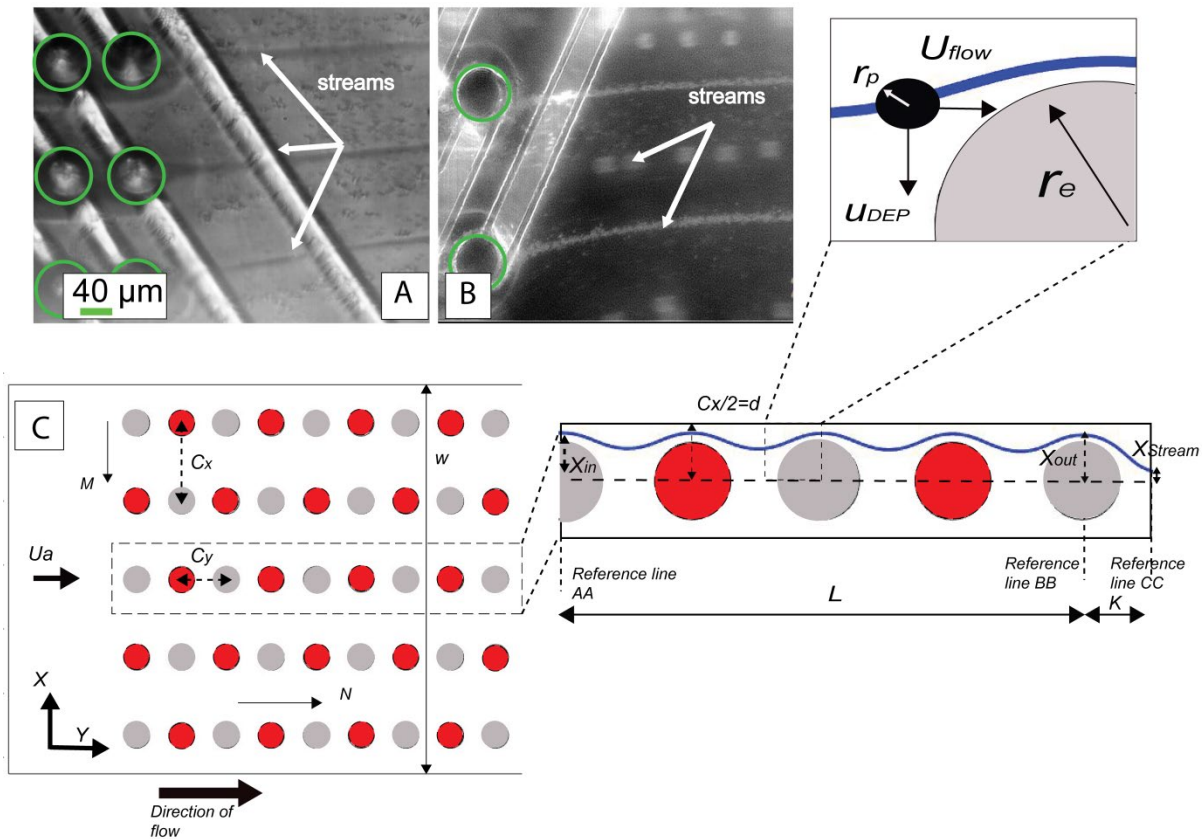


Figure 1. A) StreamingDEP behavior of *Candida albicans* cells when using an array of 3D carbon electrodes (green circles), polarized using a sinusoidal with frequency 500 kHz, magnitude 20Vpp, contained in a micro-channel. Flow velocity was 0.022 m/s due to a flow rate of 100 ul/min and a channel cross-section of 600 μm by 100 μm. B) Continuous separation of 1 and 10 μm by streaming small particles around regions of high field gradient around electrodes (green circles) using streamingDEP, and focusing big particles to regions of low field gradient in between electrodes using negativeDEP. Array was polarized at 100 kHz and 20Vpp and a flow velocity of 0.022 m/s was used. C) Schematic of an electrode array contained

in a microfluidic channel detailing terms and nomenclature used in this work, see text for details and supplementary information for a table listing all variables used here. The region of analysis (ROA) is shown in the inset. Note the illustration of a hypothetical particle trajectory shown in blue solid line.

Owing to the nature of the pressure-driven flow assumed here, the flow velocity in the channel will have a 3D parabolic profile as previously characterized by other authors [36]. The flow in the ROA is assumed fully developed, laminar, steady and incompressible. By adopting Poiseuille flow between stationary boundaries, the maximum velocity occurs at the middle between electrode surfaces in the X-Y plane and at mid-channel height $H/2$ in the Y-Z plane. We assume a Reynolds number $Re \leq 10$ which is representative of flowing aqueous media in most microfluidics-based DEP devices [37,38]. At $Re < 10$, the creation of vortices in the domain can be neglected based on the work by Ming-Hsunwu et al [39]. Based on the work by previous authors and the gap to electrode diameter ratios explored here, we also assume there are no vortices formed between the cylindrical electrodes [40,41] and that the electrodes do not disturb the flow pathlines [36]. Table S1 in the supplementary information describes all variables used in this analysis.

Three reference lines parallel to the X axis will be used here to facilitate analysis: 1) line *AA* intersecting the center of the first electrode of the row of interest, 2) line *BB* intersecting the center of the last electrode, and 3) line *CC* at a distance K away from *BB* (see inset of figure 1C). The location in which the particle enters the ROA at line *AA* is given by X_{in} and can be any position between the edge of the first electrode and the middle of the gap between rows, or $r_e < X_{in} < C_x/2$. The length of the electrode row, or distance between *AA* and *BB*, will be given by $L = (NC_y)$. The location of the particle at the line *BB* will be given by X_{out} and is used here as an auxiliary variable to relate X_{out} to X_{stream} (see supplementary information S2). X_{stream} is the final position of the particle and is measured along the line *CC*. Accordingly, the width of streams obtained with streamingDEP would be $2X_{stream}$. Stream width is assumed to be a parameter to be selected by the designer.

Several variables are defined to make this analysis non-dimensional. All normalized variables are denoted by an asterisk. For example, any distance in the X axis as well as X_{in} , X_{out} and X_{stream} are rendered non-dimensional by dividing each by $d = (C_x/2)$ leading to X_{in}^* , X_{out}^* , and X_{stream}^* (i.e. $X_{in}^* = X_{in}/d$). Distances in the Y axis are similarly divided by L . Other defined variables are confinement ratio $\lambda = r_p/d$ and constriction ratio $\gamma = r_e/d$. The confinement ratio enables the comparison between the gap between electrodes and the particle size. As the confinement ratio approaches 1, the particle size would be

comparable to the electrode gap and the presence of such a particle could affect the flow and electric fields. The constriction ratio enables the comparison of electrode size to the separation between the electrodes. Constriction ratios close to 1 imply that the electrode size is comparable to the gap, which can affect the electric field in the region. Values of γ close to 1 can also affect the flow in the electrode array as the curvature of the electrode will play an important role in determining the flow profile.

2.3 Derivation of streamingDEP number (SDN)

A particle that enters the ROA at a given X_{in} can have three outcomes: 1) trapped, 2) streamed under the influence of DEP force, or 3) eluted without any influence from the DEP force. Here the particle is defined to undergo streaming if it reaches the calculated focusing distance of X_{out} along the X axis before the time it takes to travel the distance L along the Y axis. Trapping will represent the case when a particle takes less time to travel the distance $X_{out} - X_{in}$ along the X axis than to travel the distance L along the Y axis, while elution will be the case when the time for the particle to travel from $X_{out} - X_{in}$ is more than the time take by the particle to travel the distance L along y axis. Hence, to be streamed the particle should satisfy the inequality,

$$\int_{X_{in}}^{X_{out}} \frac{dx}{u_{px}} \leq \int_0^L \frac{dy}{u_{py}} \quad (1)$$

where the left side of the inequality describes the time taken by the particle to cover the distance from X_{in} to X_{out} at a velocity magnitude given by u_{px} in the X axis and the right side describes the time taken to cover the length L along the Y axis at the magnitude of velocity given by u_{py} . Of note, X_{in} is taken at reference line *AA* while X_{out} is taken at reference line *BB*.

A particle with radius r_p in the ROA will be subjected to the influence of different forces. Drag due to flow in the channel and DEP due to polarization of the electrode array are emphasized here. Although the particle will sediment, this will be considered negligible here since the sedimentation distance is significantly less than the motion in X-Y in the time the particle resides in the channel. Lift forces are also considered negligible since the DEP force in this domain is at least 10 times larger than the lift forces, as calculated using the procedure reported by other authors [42,43]. The DEP force \vec{F}_{DEP} acting on a spherical particle as those assumed here is given by equation 2 and depends on the radius of the particle r_p , the gradient of the square of the electric

field $\nabla \vec{E}_{rms}^2$, permittivity of the media ϵ_m and $Re[f_{CM}]$, which is the magnitude of the real part of the Clausius-Mossotti factor f_{CM} . This factor is given by equation 3 where ϵ_p^* and ϵ_m^* denote the complex permittivity of particle and media respectively, σ denotes the conductivity of particle or media, i represents the imaginary number $\sqrt{-1}$, and f represents the frequency of the polarizing signal.

$$\vec{F}_{DEP} = 2\pi r_p^3 \epsilon_m Re[f_{CM}] \nabla \vec{E}_{rms}^2 \quad (2)$$

$$f_{CM} = \frac{\epsilon_p^* - \epsilon_m^*}{\epsilon_p^* + 2\epsilon_m^*} \text{ where, } \epsilon^* = \epsilon + \frac{i\sigma}{2\pi f} \quad (3)$$

The Stokes drag force \vec{F}_{DRAG} is given by equation 4 where the dynamic viscosity of the media is μ , the flow velocity throughout the ROA is \vec{U}_{flow} and the particle velocity \vec{u}_p . For convenience throughout this analysis, the terms pertaining to particle velocity are assigned lowercase letter u whereas the terms pertaining to flow velocity are indicated by uppercase U .

$$\vec{F}_{DRAG} = 6\pi\mu r_p (\vec{U}_{flow} - \vec{u}_p) \quad (4)$$

Hence, according to Newton's second law of motion, the trajectory of the particle in the ROA is influenced by the total force, which is calculated by vector summation of \vec{F}_{DEP} and \vec{F}_{DRAG} :

$$m_p \frac{d\vec{u}_p}{dt} = \vec{F}_{DRAG} + \vec{F}_{DEP} \quad (5)$$

where the mass of the particle is m_p . After proper manipulation [17], the particle velocity is obtained as,

$$\vec{u}_p = \vec{U}_{flow} + \frac{\vec{F}_{DEP}}{6\pi\mu r_p} = \vec{U}_{flow} + \vec{u}_{DEP} \quad (6)$$

Where the magnitude of the particle velocity vector in the X axis is denoted by u_{px} and that in Y as u_{py} . \vec{u}_{DEP} is the component of velocity resulting due to the effect of DEP force.

Once particle velocity \vec{u}_p is defined, important assumptions to define u_{px} and u_{py} are necessary. In the absence of the DEP force and with lift forces assumed negligible here, the particle does not face displacement along the X-axis. Thus, the X_{in} and X_{out} are expected to remain the same. Under the influence of positive DEP, the particle is attracted towards the electrodes and moves towards them. Thus, X_{out} is expected to be smaller than X_{in} under the action of DEP force. Since the displacement along X axis occurs only due to DEP force, the magnitude of the velocity of the particle in the X axis, or u_{px} , is only due to the DEP velocity of the particle as shown in equation 7

$$u_{px} = U_{flowx} + u_{DEPx} \approx u_{DEPx} \quad (7)$$

Since u_{DEPx} depends on the electric field, computational modeling with COMSOL Multiphysics was used to derive a non-dimensional expression for

the electric field E^* as previously reported by Kralj, et. al and Schnelle, et al. [44,45]. The expression for E^* is reported as equation 8 (details on its derivation are presented as supplementary information, section S3)

$$E^* = 0.55 \left(\frac{X^*}{\gamma}\right)^{-1} \quad (8)$$

where $X^* = x/d$ and x is the distance between the point of analysis and the center of the electrode. E_{rms} corresponds to the root mean square value in an AC sinusoidal signal like those used in this work and is defined as $E_{rms} = 0.7E$, which can be further written in terms of the non-dimensional electric field E^* as;

$$E_{rms} = \left(\frac{0.7V^*E^*}{(d-r_e)\sqrt{\gamma}}\right) \quad (9)$$

In the Y axis, the situation reverses when compared to that described for the X axis. In the Y axis, particle movement will mainly occur due to flow velocity U_{flowy} since u_{DEPy} is around 10^4 times smaller than the flow velocity component (see supplementary information, section S4). Hence,

$$u_{py} = U_{flowy} + u_{DEPy} \approx U_{flowy} \quad (10)$$

Although the magnitude U_{flowy} will vary throughout the ROA due to flow expansion and constriction along the electrode array, here we simplify the analysis by determining the flow profile between the narrowest gap between electrodes depending on the location of the particle X_{in}^* but at a constant position in the Y axis. The 2D parabolic profile of the magnitude U_{flowy} at the reference line AA , or BB , in an arbitrary X-Y plane at height h is obtained using equation 11 when considering the flow between two stationary parallel plates, or the electrode boundaries (see supplementary information section S5 for details on its derivation).

$$U_{flowy} = \frac{12U_a(h/H)(1-h/H)(w/d)(X_{in}^* - \gamma)(2 - \gamma - X_{in}^*)}{M(1-\gamma)^3} \quad (11)$$

Where γ is the constriction ratio given by r_e/d ; U_a is a design parameter representing the average flow velocity in the channel before the electrode array, and can be calculated using the cross-sectional area of the channel and the flow rate at the same plane of the ROA; the term $(h/H)(1 - \frac{h}{H})$ enables the calculation of U_{flowy} at height h ; $\left(\frac{w}{d}\right)$ represents the normalized width of the channel; and M is the number of electrode rows in the channel. Importantly, the magnitude U_{flowy} given by equation 11 is at a constant Y position. Thus, the right side of the integral in equation 1 is reduced to a simple expression of the form distance/velocity. By

considering the maximum velocity in the ROA and assuming this value constant throughout the domain, the time calculated for a particle to traverse L would be the least possible time for streaming.

Obtaining a non-dimensional variable for the magnitude of velocity is important for deriving a general equation of velocity in the domain and enabling its use for different flow rates and electrode diameters. The magnitude of particle velocity in both axes u_{py} and u_{px} can be non-dimensionalized by dividing by U_a leading to equations 12 and 13,

$$u_{py}^* = \frac{u_{py}}{U_a} \quad (12)$$

$$= \frac{12(h/H)(1-h/H)(w/d)(X_{in}^* - \gamma)(2 - \gamma - X_{in}^*)}{M(1 - \gamma)^3}$$

$$u_{px}^* = \frac{u_{px}}{U_a} = \frac{2\pi\epsilon Re[f_{CM}]r_p^3 \nabla \vec{E}_{rms}^2}{6\pi\mu r_p U_a} \quad (13)$$

And both sides of the inequality in equation 1 can be transformed to non-dimensional terms by using equations 2-13 and the fact that $dx^* = \frac{dx}{d}$ and $dy^* = \frac{dy}{L}$ to yield equation 14, where the right side is shown as a constant value when considering a uniform u_{py} through the ROA as detailed above,

$$\int_{X_{in}^*}^{X_{out}^*} \frac{d * dx^*}{U_a u_{px}^*} \leq \frac{L}{U_a u_{py}^*} \quad (14)$$

The component of $\nabla \vec{E}_{rms}^2$ in the X axis is calculated by taking the derivative of E_{rms}^2 (from equation 9) with respect to X. By calculating $\nabla \vec{E}_{rms}^2$ and substituting the value for magnitude of u_{px}^* and u_{py}^* as stated in equations 12 and 13, equation 14 can be re-written as equation 15.

$$\int_{X_{in}^*}^{X_{out}^*} \frac{3\mu * d * (d - r_e)^2 x^3 dx^*}{\epsilon Re[f_{CM}]r_p^2 (-0.29)V^2 r_e d} \quad (15)$$

$$\leq \frac{12U_a \left(\frac{w}{d}\right)(h/H)(1-h/H)(X_{in}^* - \gamma)(2 - \gamma - X_{in}^*)}{\lambda^2 \epsilon Re[f_{CM}]V^2 \gamma}$$

After integrating with respect to x^* on the left side, and using the substitution $\lambda = r_p/d$ for confinement ratio, the following inequality is obtained;

$$\frac{2.58\mu(X_{in}^{*4} - X_{out}^{*4})(d - r_e)^2}{\lambda^2 \epsilon Re[f_{CM}]V^2 \gamma} \leq \frac{L}{u_{py}^* U_a} \quad (16)$$

Where u_{py}^* is given by equation 12 and not substituted for the sake of conciseness. Moreover, equation 16 can be simplified by transferring all the terms from the right-hand side to the left and substituting $L = NC_y$. Of note, all the terms in equation 16 are greater than or equal to zero when positive DEP is present. This can be further expressed as;

$$0 \leq \frac{2.58\mu(X_{in}^{*4} - X_{out}^{*4})(d - r_e)^2 u_{py}^* U_a}{\lambda^2 \epsilon Re[f_{CM}]V^2 \gamma NC_y} \leq 1 \quad (17)$$

Where the term $\frac{2.58\mu(X_{in}^{*4} - X_{out}^{*4})(d - r_e)^2 u_{py}^* U_a}{\lambda^2 \epsilon Re[f_{CM}]V^2 \gamma NC_y}$ is the

Streaming DEP Number (SDN) and depends on the device geometry, particle properties and the profiles of both the flow and electric fields in the domain. SDN can be used to predict the streaming behavior for a particle that enters the channel at a given X_{in} , based on the design parameters. SDN=0 when no flow is present. SDN>1 signifies that the time taken by the particle to reach the outlet is too short for streaming. $0 < SDN \leq 1$ represents streaming since the time taken by the particles to travel in x direction to the location X_{out}^* is smaller than the time taken by the particles to travel the distance of $L (=NC_y)$ in y direction. However, this condition also applies to particles that are trapped. Hence, distinguishing between the streaming and captured particles based on the value of SDN alone has limitations. Although further modeling of SDN could be done by determining the probability of the injected cells reaching the outlet, the number of cells entering the system will not be known *a priori* in most applications. Hence, experimentation was conducted to elucidate the transition between trapping and streaming under experimental parameters yielding a $0 < SDN \leq 1$.

3. Experimental materials and methods

3.1 Experimental device

Here we used 3D carbon-electrode dielectrophoresis (carbonDEP) [32,31,46-49,34,50-52] devices featuring carbon microelectrodes inside a polymer microchannel. The fabrication procedure has been detailed several times before [31,51,35,53]. Briefly, micro pillars were fabricated by a two-step photolithography process of SU-8 (Gersteltec, Switzerland), a negative-tone photoresist, on a silicon wafer substrate. These structures were then carbonized by heat treatment to 900 °C in a furnace with inert atmosphere. The experimental device featured an electrode array of 180 columns and 5 rows. Individual electrodes were 100- μ m high and 50 μ m-in diameter. The separation between the centers of the electrodes in the X-axis (C_x) was 122 μ m, while C_y was 105 μ m. A thin layer of SU-8 was then fabricated to insulate the planar connecting leads and to planarize the channel bottom. A 0.6 mm-wide, 3 cm-long channel was cut from a 127 μ m-thick double sided pressure sensitive adhesive, or PSA (Switchmark 212R, Flexcon, USA) and manually adhered to a drilled acrylic holder, following a process

described elsewhere [54]. This arrangement was then manually positioned around the carbon electrode array and sealed by using a rolling press.

3.2 Experimental samples

Three different experimental samples were used: 1) a suspension of 1 μm -diameter particles 2) a mixture of 1 and 10 μm particles in equal parts and 3) a suspension of *C. albicans* cells.

1 μm polystyrene beads were purchased from Bangs Laboratories (PS04001lot no. 9396) while 10 μm beads were acquired from Magsphere (catalog no. PS010UM). Particle suspensions were prepared in distilled water supplemented with 0.1% Bovine Serum Albumin (BSA, Sigma Aldrich A7906) by weight to a particle concentration of around 10^6 per ml and electrical conductivity of $1 \cdot 10^{-5}$ S/m. The viscosity μ of the media was that of water at room temperature (0.00089 Pa·s). The conductivity of the latex particles was assumed as 0.0052 S/m with surface conductance of $1.5 \cdot 10^{-9}$ S [55]; and relative permittivity of 2.5.

C. albicans cells (ATCC 18804) were cultured in yeast malt broth (YMB) (Sigma Aldrich Y3752) with 5% sugar solution for 24 hours. The average cell size for *C. albicans* was 4-5 μm . The sugar solution was prepared with 200 ml distilled water by adding 18 gm sucrose, 0.5 g dextrose and 0.3 g Bovine Albumin Serum. The conductivity of the sugar solution was ~ 20 $\mu\text{S}/\text{m}$. The cell culture for DEP was prepared by centrifugation, washing and resuspension of the cell sample with the sugar solution at least thrice with the final cell concentration of approximately $\sim 10^7$ cells/ml. The dielectric parameters that would allow for modeling the DEP behavior for *C. albicans* cells are not currently available in the literature. However, the behavior of *C. albicans* has been shown to be similar to that of *S. cerevisiae* [56,57], a well-studied strain in the context of DEP [58,59]. Thus, the dielectric parameters of *S. cerevisiae* are assumed to be a good approximation for *C. albicans* in this work.

3.3 Experimental protocol

The experiments with 1 μm particles were carried out by varying the flow velocity, frequency of current and voltage. One parameter was varied at a time whereas the other two were held constant. A syringe pump (FusionTouch 200, Chemyx, USA) was used to implement a specific flow velocity in the range 0.016-0.088 m/s. The voltage in the domain was varied from 10 to 20 V peak to peak (V_{pp}) and the frequency was varied from 10 kHz to 10 MHz (using a BK Precision 4052 Function Generator, USA). Experiments were recorded using a Nikon Eclipse LV100 equipped with

a fast camera (Andor Zyla). Initially the channel was entirely filled with the experimental sample and the electric signal was switched on only after a steady flow was established. Of note, the voltage drop across carbon electrodes is influenced by the resistivity of the carbon used here ($\sim 1 \cdot 10^{-4}$ $\Omega \cdot \text{m}$ [60]). Based on previous analysis of this particular electrode design [31], we considered a voltage drop of 25% at the surface of the microelectrodes compared to that delivered by the function generator. The voltage values reported in this work are the peak to peak values of the sinusoidal signal delivered by the function generator.

The experiments with *C. albicans* cells were carried out in a way similar to that just described. Only the polarization voltage was selected as a variable in these experiments and ranged from 8 to 20 V_{pp} . The flow rate for these experiments was held constant at 0.056 m/s and the frequency selected for trapping was 500 kHz since previous results showed how *C. albicans* displayed positive DEP force at this frequency [61].

3.4 Data analysis

The image stacks recorded during experiments were analyzed using ImageJ software. We monitored the signal intensity at a line 250 μm way from the last column in the electrode array where the electric field did not affect the particle streaming anymore. Peaks on the signal intensity plot denoted particle streams. At least 3 experimental measurements were obtained for a given data point, i.e. specific flow rate, polarization voltage and field frequency, and all were normalized against a control value for such data point. Controls were obtained when implementing the same experimental conditions but without turning the electric field on. Moreover, the streamwidth reported is that measured at the exit of the centermost electrode row, in the ROA described above to avoid the effect caused by the channel boundaries. The resolution of the measurement is limited by the microscope imaging system, which was 0.1 μm . Of note, this method allowed to characterize differences in signal intensity but did not allow quantifying the particle concentration in the streams. Instead, we studied five representative cases of SDN where at least 60, 70, 80, 90 and 100% of the particles in the selected domain form focused streams. This was implemented by assuming different values of $X_{in}^* = 0.6, 0.7, 0.8, 0.9$ and 1. These were used as guidelines for particle trapping. For example, if a particle enters the domain at $X_{in}^* = 0.8$ and exists at certain X_{stream}^* value, all the particles entering the domain with a smaller X_{in}^* will elute at a distance smaller than X_{stream}^* .

. $X_{in}^* = 1$ encompasses the behavior of 100% of the particles.

4. Experimental results

4.1 Effect of flow rate

For the 1 μm polystyrene particles, streaming was observed in the X-Y plane at height h of around 20 μm . This height was determined by measuring the travel of the microscope along the Z axis during focusing at the height where streams are visible. The plane of the microscope image was fixed at this height for the entire set of experiments. SDN values were calculated for different flow rates using equation 17 and were seen to increase with the increase in flow rate. Particle streaming and the generation of particle streams of various widths was evident in the flow velocity range 0.016-0.088 m/s as illustrated in figure 2A. The shaded regions are used to indicate different zones, namely capture, streaming due to DEP, and elution without the effect of DEP as observed in the experiments. For example, the flow rates up to 0.016 m/s show capture behavior according to the experiments.

Streaming behavior was first observed at the flow velocity of 0.016 m/s. The streamwidth rapidly increased as the flow velocity increased to 0.022 m/s.

At this velocity, the SDN value for $X_{in}^* = 1$ was 0.75 and it met the constraint for particle streaming. The intensity of the stream recorded at this velocity was the highest among all data recorded in this set of experiments, as seen in figure 2B. As the velocity increased further, the streamwidth increased but the stream intensity decreased. The data point for velocity of 0.066 m/s shows the lowest stream intensity. At this velocity, the SDN value for $X_{in}^* = 1$ and $X_{in}^* = 0.9$ is greater than 1, which implies that the particles entering the domain at these inlet points would no longer form streams. The $X_{in}^* = 0.8$ has an SDN value of 0.9 implying that particles entering the channel at this point would form streams. Beyond the flow rate of 0.066 m/s, streams were not visible in the experiment. For flow rates greater than 0.070 m/s, the SDN value for $X_{in}^* = 0.8$ is greater than 1, implying these particles were no longer streamed. The SDN value for $X_{in}^* = 0.7$, is around 0.5, but no streams were visible at this flow rate. Streams were also not visible for SDN values below 0.5, which could imply that the particles at such SDN values were captured. Although the streamwidth was seen to increase with an increase in flow rate, it only varied by 3-4 μm . Nevertheless, in the context of the particles used here (1 μm -diameter), a wider streamwidth meant that more particles were being streamed. Unfortunately, the increase in number of streamed particles could not be quantified due to experimental limitations.

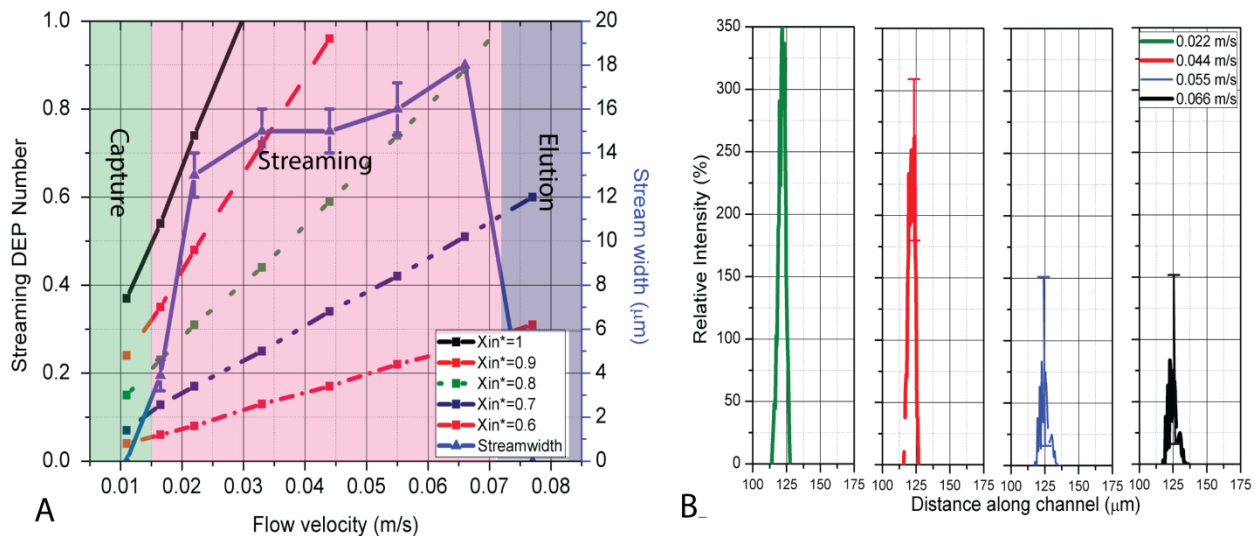


Figure 2 A) Plot of the value of streaming DEP number (SDN) for $X_{in}^* = 0.6$ to 1 and streamwidth depending on flow velocity. The SDN values increase with the flow velocity in all cases but with different slope. The shaded regions indicate the range of flow rates that show the capture, streaming or elution behavior. B) The plot of the relative intensity analysis for streams from the central electrode array for flow velocities between 0.022-0.066 m/s shows a decrease in stream intensity as flow velocity increases.

4.2 Effect of voltage

The value of SDN was calculated for different voltages and shown to decrease with increasing voltage (figure 3A). This was expected as the DEP force increases proportional to the voltage. However, stream formation was only obtained in the voltage range from 12-20V. Voltages beyond 20 V could not be explored due to experimental limitations.

At 10 V, the SDN value for $X_{in}^* = 0.8$ and above was greater than 1 which would mean particles would not form streams. As the voltage increased, streaming

became visible. At 12 V, streams with low intensity (figure 3B) were recorded. At such voltage, the SDN value for $X_{in}^* = 0.8$ was 0.85, and these particles were expected to show streams. At 20 V, the stream intensity was maximum and the SDN value for $X_{in}^* = 1$ was below 1, resulting in the bulk of particles showing streaming and thus the strong intensity peak. Based on the observations made here, streaming was clearly visible for SDN values greater than 0.6, i.e. streaming was prominent when SDN values for $X_{in}^* = 1$ was between 0.6-1.

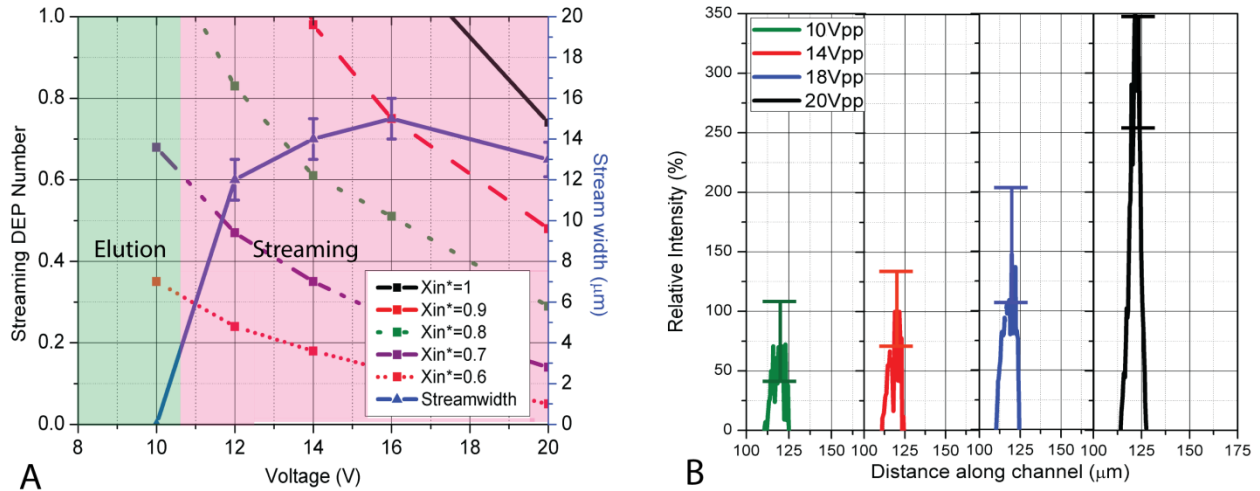


Figure 3 A) The value of streamwidth with the change in voltage is plotted along with the calculated SDN values for $X_{in}^* = 0.6$ to 1. The SDN values and streamwidth decrease with the increasing voltage. The shaded regions indicate the range of voltage showing elution, streaming and capture behaviors. B) Intensity analysis for streams obtained at different voltages. The intensity of stream increases with the increase in voltage.

4.3 Effect of frequency

The SDN values for different frequencies are plotted in figure 4A. The SDN value for the different X_{in} values increased with the increase in frequency. The behavior of the latex particles in response to frequency is determined by the value of the real part of Clausius Mossotti factor $Re[f_{CM}]$. In the case of 1 μm latex particles and the experimental conditions used here, particles were expected to exhibit positive DEP at frequencies up to 1 MHz and then transition towards negative DEP in the frequency range of 1 to 20 MHz (see supplementary information S5). Figure 4B shows an increase in stream intensity that was

proportional to frequency. At 250 kHz, a peak in stream intensity was observed, and intensity then decreased with an increasing frequency. With an increase in frequency beyond 250 kHz, the SDN value for $X_{in}^* = 1$ increased beyond 1, indicating that streams would not be formed for particles originating at this point. At the frequency of 1 MHz, the SDN value for $X_{in}^* = 0.9$ is 0.9, whereas the SDN value for $X_{in}^* = 0.8$ is 0.5. Streams were visible at this frequency. Such behavior reinforced the fact that particles seemed to stream only when the SDN values for a given X_{in} were greater than ~ 0.6 and that stream intensity was higher as the X_{in} number approached 1.

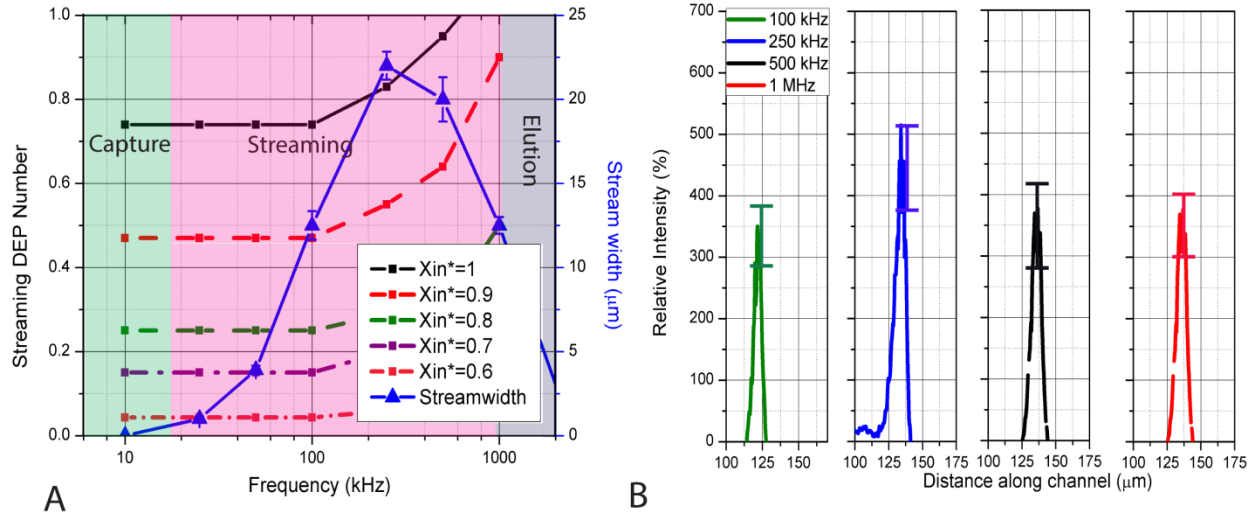


Figure 4 A) Plot of the SDN value for different values of X_{in} and streamwidth for increasing frequency values. Streaming behavior increases with increase in frequency up to 250 kHz and decreases with further increase in frequency. The shaded regions show the experimentally determined capture, streaming and elution zones. These show the ranges of frequency which show the indicated behavior. B) The plot shows the relative intensity of the stream at different frequencies. The intensity increases with increase in frequency to 250 kHz and decreases with further increase.

4.4. StreamingDEP of *Candida albicans* cells

C. albicans is a yeast common in the human gut flora that can become an opportunistic pathogen in immunocompromised individuals [62]. It is one of the most prevalent causes [62] of systematic candidiasis, or candida infection, leading to a mortality rate as high as 40% [63]. Since the use of traditional cell culture to identify the presence of *C. albicans* in a sample yields delayed results, an assay to rapidly assess the presence of this yeast can have tremendous impact on the timely and correct treatment of candidiasis. To this end, here we present initial characterization of the streamingDEP behavior of *C. albicans* towards a future diagnosis assay using continuous sorting.

Figure 5 shows the stream widths obtained for *C. albicans* using different voltages in the range 8-20 V_{pp} at the frequency of 500 kHz. This frequency was used due to previous results showing positive DEP behavior of *C. albicans* at such value [61]. Due to the lack of studies of the dielectric parameters of *C. albicans* in the literature, their DEP behavior was approximated to that of *S. cerevisiae* following the work by previous authors [56,57]. Under the experimental conditions used here, the $\text{Re}[f_{CM}]$ for *C. albicans* was approximated as 0.65 (details in supplementary information section S6) and such value was used to calculate the SDN numbers reported in this section. At 10 V_{pp} , the stream width is

around 25 μm as seen in figure 5A, but the corresponding stream intensity in figure 5B is the lowest. This indicates that though streaming is observed, not all particles are being streamed. This is confirmed by the fact that SDN when $X_{in}^*=1$ is greater than 1. At the voltage of 14 V_{pp} , both the streamwidth and the stream intensity obtained were high, indicating that large numbers of cells are focused at this voltage. As indicated in figure 5A, the SDN value for all X_{in}^* values in this case is also less than 1 and thus cells entering the domain at all the distances X_{in}^* are expected to form streams.

At higher voltages, the SDN value for the cells decreases further. The streamwidth and stream intensity also decreases with the increase in voltage. This behavior can be attributed to cell capture rather than streaming. Smaller values of SDN imply particle capture rather than streaming. Though the cells and particles used here exhibit different dielectrophoretic properties, both the species show evidence of streaming. The streaming behavior could be tailored by changing the system parameters. Due to difference in structure and surface, the cells and particles are expected to show different reflected intensities and thus different stream intensities. However, the trend in the streaming behavior observed is comparable. The relationship between SDN and streaming behavior in case of the cells is similar to the behavior observed for the latex particles.

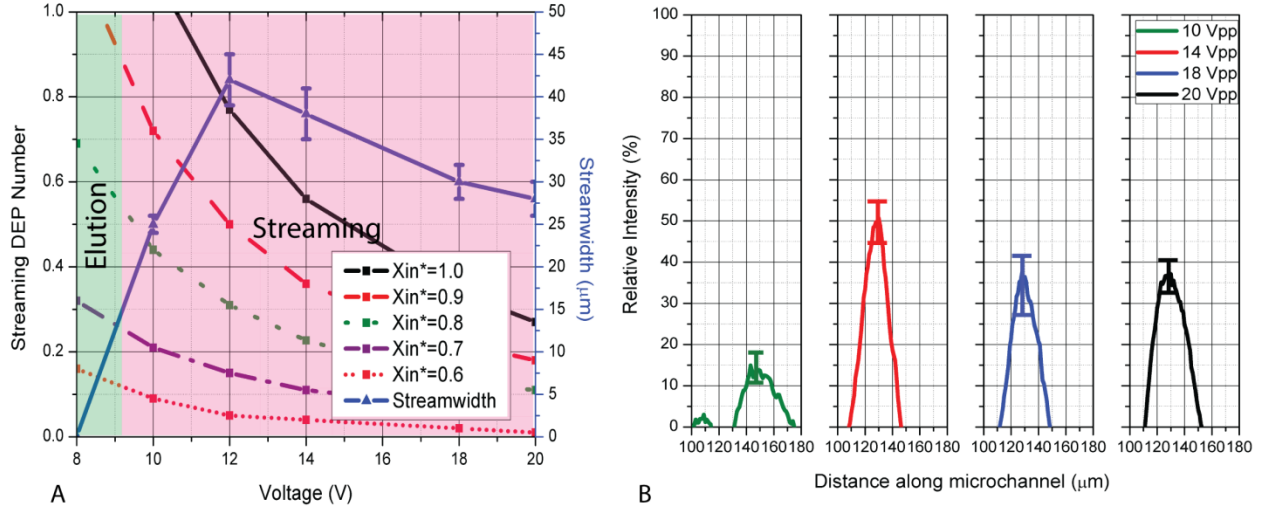


Figure 5 A) The plot shows the SDN values calculated for *C. albicans* at different voltages and X_{in}^* values, with the flow and field frequency held constant at 0.056 m/s and 500 kHz respectively. The SDN for 10 V is greater than 1 and no streaming behavior is expected at this voltage for particles starting at $X_{in}^* = 1$. However, streaming can be seen for the particles starting at $X_{in}^* = 0.9$ and lower. As the voltage increases, the SDN value for all X_{in}^* values decreases gradually. The streamwidth also decreases with the increase in voltage. The shaded regions show the range of voltages in each of the two zones capture and streaming due to DEP. Voltage values >20 V were not explored due to experimental limitations. B) The plot in this figure shows the change in intensity with respect to the change in voltage. At 10 V, the stream intensity obtained is low. This intensity increases with increase in voltage to 14 V. However, the intensity decreases when using voltage values >14 V. This decrease in intensity corresponds to the decrease in the value of SDN at higher voltages. See text for further details.

5. Discussion

1 μm latex beads and *C. albicans* cells showed positive DEP in all frequencies used in this study. When the DEP force dominated, the particles were captured at the electrodes by positive DEP. As the flow velocity increased, the particles and cells ceased to trap and began to flow along the vicinity of the electrodes forming streams. As the flow velocity increased further, the drag force became dominant and the particles eluted without any influence of DEP. Based on this phenomenon, three zones were defined: 1) capture zone, indicating particle trapping due to DEP, 2) streaming zone indicating formation of streams due to combined action of DEP and drag forces, and 3) elution zone, when particles flow out of the microchannel without any effect of DEP. StreamingDEP was observed for SDN values lower than 1 but higher than 0.6 for all values of X_{in}^* (the relative location where particles enter the region of analysis). SDN values < 0.6 seem to yield particle capture. Particle elution was observed when $\text{SDN} > 1$. These results are expected to be applicable to any spherical particle with dielectric properties, including cells, since the SDN postulated here is dependent on the given values of the Clausius Mossotti factor and the radius of any particle of interest. However, the velocity profile along the channel height is expected

to change with h within the channel. In the experiments conducted here, the analysis focused on a fixed height in the channel. Given the parabolic profile of the flow velocity in the channel, the maximum velocity in the vertical plane will occur at half the channel height, or $H/2$. This will be important when calculating the parameters to obtain streaming of a given particle so that optimized values are chosen that enable particle streaming throughout the entire height of the channel and not only specific planes. Such consideration will yield higher specificity and efficiency during separation of a targeted particle or cell from its background.

The throughput of cell separation using streamingDEP will largely depend on the width of the stream. A wider stream is likely to be desired to maximize throughput. However, the stream can also be tailored in width to facilitate continuous retrieval of the targeted cells using funnel geometries at the end of the array. For example, thin streams may be desired in case of devices with restricted footprint. The importance of a SDN that characterizes this system of continuous separation is precisely the capability to dictate the width of the stream depending on the system variables. The SDN can be calculated for a range of particle input locations X_{in}^* once the streamwidth is selected and using the

system and cell properties. System variables include flow velocity, and both frequency and magnitude of the signal polarizing the electrode array. Cell properties include its electrical polarizability given by its membrane capacitance and size. Beyond designing the system to achieve a specific streamwidth, the SDN can also enable the control of the mode of operation of a given electrode array by activating trapping, streaming or elution. Further control could be implemented by controlling X_{in}^* by using other label-free techniques for cell focusing such as inertial microfluidics. In such case, a coarse cell separation based on size could be achieved prior to feeding these cell streams to a streamingDEP array to enable finer separation using membrane capacitance.

In the experimental setup used here, the particle dimensions were much smaller than the scale of the electric field gradient. For a device designed to separate bigger cells that have dimensions comparable to the electrodes used here, the presence of particles can alter the charge density around the electrode [65] and the effect of this on the electric field will thus need to be considered. If possible, a preferred course of action would be to increase the size of the gap between electrodes. Cell adhesion or formation of particle chains around the electrodes [66] can also affect the DEP force acting on the particles approaching the electrode, which may affect their streaming behavior. Correction factors have been introduced by other authors to account for these perturbations [24,67] and ongoing work is on studying the applicability of such factors in our system. An important feature of the system presented here is the generation of as many streams as rows in the array. Hence, one can envision a high throughput system with many rows and funnel-like geometries neatly aligned to enable continuous particle retrieval from the channel. However, the presence of channel walls can affect the position of the streams exiting the electrode array. Such effect is already observed at the

outermost rows, where the particle streams are pushed towards the middle of the channel due to the expansion of the flow at the exit of the electrode array. Thus, the channel wall should be designed, i.e. expanding at the exit of the array, such that it does not affect the flow profile and the location of the streams in the device. If the channel walls are close to the electrode rows, near-wall effects can also cause the velocity of the particle to reduce and corresponding correction factors will need to be introduced. Lastly, the shape and geometry of the electrodes is expected to have a measurable impact on the formation of streams as previously observed by us in computational modeling [30]. Ongoing work is on elucidating the effect of electrode shape on the generation and characteristics of streams.

6. Conclusion

Here we contributed an analytical expression of a Streaming DEP Number or SDN that relates the width of the particle or cell stream, originated due to the equilibrium between drag and DEP forces acting on the particle or cell, to different system parameters and properties of the particle or cell of interest. SDN values obtained for streamingDEP with both latex particles and *Candida albicans* cells were used to validate such streaming behavior. Based on these studies, the range of SDN values 0-0.6 imply particle capture due to DEP, values in the range 0.6-1 indicate streaming due to DEP, and values beyond 1 indicate particle elution without an influence of DEP force. This is important because SDN can serve as a tool to design DEP devices that yield specific streaming behavior of a desired cell or particle. Ongoing work is on the effect of electrode geometry, wall effects and particle agglomerates on the SDN.

Conflict of Interest

The authors declare no conflict of interest

References:

- [1] J. Kruger, K. Singh, A. O'Neill, C. Jackson, A. Morrison, P. O'Brien, Development of a microfluidic device for fluorescence activated cell sorting, *J. Micromechanics Microengineering*. 12 (2002).
- [2] J.C. Baret, O.J. Miller, V. Taly, M. Ryckelynck, A. El-Harrak, L. Frenz, C. Rick, M.L. Samuels, J.B. Hutchison, J.J. Agresti, D.R. Link, D.A. Weitz, A.D. Griffiths, Fluorescence-activated droplet sorting (FADS): Efficient microfluidic cell sorting based on enzymatic activity, *Lab Chip*. 9 (2009) 1850–1858. doi:10.1039/b902504a.
- [3] A.Y. Fu, C. Spence, A. Scherer, F.H. Arnold, S.R. Quake, A microfabricated fluorescence-activated cell sorter., *Nat. Biotechnol.* 17 (1999) 1109–11. doi:10.1038/15095.
- [4] J. Zeng, C. Chen, P. Vedantam, V. Brown, T.-R.J. Tzeng, X. Xuan, Three-dimensional magnetic focusing of

- particles and cells in ferrofluid flow through a straight microchannel, *J. Micromechanics Microengineering*. 22 (2012) 105018. doi:10.1088/0960-1317/22/10/105018.
- [5] S. Miltenyi, W. Muller, W. Weichel, A. Radbruch, High Gradient Magnetic Cell Separation With MACS1, 238 (1990) 231–238.
- [6] D.R. Gossett, W.M. Weaver, A.J. MacH, S.C. Hur, H.T.K. Tse, W. Lee, H. Amini, D. Di Carlo, Label-free cell separation and sorting in microfluidic systems, *Anal. Bioanal. Chem.* 397 (2010) 3249–3267. doi:10.1007/s00216-010-3721-9.
- [7] J. McGrath, M. Jimenez, H. Bridle, Deterministic lateral displacement for particle separation: a review, *Lab Chip*. 14 (2014) 4139–4158.
- [8] M. Jiang, K. Budzan, G. Drazer, Fractionation by shape in deterministic lateral displacement microfluidic devices, *Microfluid. Nanofluidics*. 19 (2015) 427–434. doi:10.1007/s10404-015-1572-6.
- [9] P. Tallapragada, N. Hasabnis, K. Katuri, S. Sudarsanam, K. Joshi, M. Ramasubramanian, Scale invariant hydrodynamic focusing and sorting of inertial particles by size in spiral micro channels, *J. Micromechanics Microengineering*. 25 (2015). doi:10.1088/0960-1317/25/8/084013.
- [10] N. Nivedita, I. Papautsky, Continuous separation of blood cells in spiral microfluidic devices., *Biomicrofluidics*. 7 (2013) 54101. doi:10.1063/1.4819275.
- [11] A. Nilsson, F. Petersson, H. Jönsson, T. Laurell, Acoustic control of suspended particles in micro fluidic chips., *Lab Chip*. 4 (2004) 131–135. doi:10.1039/b313493h.
- [12] F. Guo, Z. Mao, Y. Chen, Z. Xie, J.P. Lata, P. Li, L. Ren, J. Liu, J. Yang, M. Dao, S. Suresh, T.J. Huang, Three-dimensional manipulation of single cells using surface acoustic waves, *Proc. Natl. Acad. Sci.* 113 (2016) 1522–1527. doi:10.1073/pnas.1524813113.
- [13] P.R.C. Gascoyne, J. Vykoukal, Particle separation by dielectrophoresis, *Electrophoresis*. 23 (2002) 1973–1983.
- [14] R. Martinez-Duarte, Microfabrication technologies in dielectrophoresis applications-A review, *Electrophoresis*. 33 (2012) 3110–3132.
- [15] A.K.M. Zaidi, D. Thaver, S.A. Ali, T.A. Khan, Pathogens associated with sepsis in newborns and young infants in developing countries., *Pediatr. Infect. Dis. J.* 28 (2009) S10–S18. doi:10.1097/INF.0b013e3181958769.
- [16] R. Pethig, M.S. Talary, Dielectrophoretic detection of membrane morphology changes in Jurkat T-cells undergoing etoposide-induced apoptosis, *Iet Nanobiotechnology*. 1 (2007) 2–9. doi:DOI 10.1049/iet-nbt:20060018.
- [17] E.A. Henslee, P. Crosby, S.J. Kitcatt, J.S.W. Parry, A. Bernardini, R.G. Abdallat, G. Braun, H.O. Fatoyinbo, E.J. Harrison, R.S. Edgar, K.F. Hoettges, A.B. Reddy, R.I. Jabr, M. von Schantz, J.S. O’Neill, F.H. Labeed, Rhythmic potassium transport regulates the circadian clock in human red blood cells, *Nat. Commun.* 8 (2017) 1978. doi:10.1038/s41467-017-02161-4.
- [18] J.L. Prieto, J. Lu, J.L. Nourse, L.A. Flanagan, A.P. Lee, Frequency discretization in dielectrophoretic assisted cell sorting arrays to isolate neural cells, *Lab Chip*. 12 (2012) 2182–2189. doi:10.1039/c2lc21184j.
- [19] M. Stephens, M.S. Talary, R. Pethig, A.K. Burnett, K.I. Mills, The dielectrophoresis enrichment of CD34+ cells from peripheral blood stem cell harvests, *Bone Marrow Transpl.* 18 (1996) 777–782. <http://www.ncbi.nlm.nih.gov/pubmed/8899194>.

- [20] J. Lu, C. a. Barrios, A.R. Dickson, J.L. Nourse, A.P. Lee, L. a. Flanagan, Advancing practical usage of microtechnology: a study of the functional consequences of dielectrophoresis on neural stem cells, *Integr. Biol.* 4 (2012) 1223. doi:10.1039/c2ib20171b.
- [21] C. Church, J. Zhu, G. Wang, T.-R.J. Tzeng, X. Xuan, Electrokinetic focusing and filtration of cells in a serpentine microchannel, *Biomicrofluidics*. 3 (2009) 044109–044110.
- [22] S.A. Faraghat, K.F. Hoettges, M.K. Steinbach, D.R. van der Veen, W.J. Brackenbury, E.A. Henslee, F.H. Labeed, M.P. Hughes, High-throughput, low-loss, low-cost, and label-free cell separation using electrophysiology-activated cell enrichment, *Proc. Natl. Acad. Sci.* 114 (2017) 4591–4596. doi:10.1073/pnas.1700773114.
- [23] I. Doh, Y.H. Cho, A continuous cell separation chip using hydrodynamic dielectrophoresis (DEP) process, *Sensors Actuators, A Phys.* 121 (2005) 59–65. doi:10.1016/j.sna.2005.01.030.
- [24] K.H. Kang, Y. Kang, X. Xuan, D. Li, Continuous separation of microparticles by size with direct current-dielectrophoresis, *Electrophoresis*. 27 (2006) 694–702. doi:10.1002/elps.200500558.
- [25] E.B. Cummings, A.K. Singh, Dielectrophoresis in Microchips Containing Arrays of Insulating Posts: Theoretical and Experimental Results, *Anal. Chem.* 75 (2003) 4724–4731.
- [26] E.B. Cummings, Streaming dielectrophoresis for continuous-flow microfluidic devices, *IEEE Eng. Med. Biol. Mag.* 22 (2003) 75–84. http://infolink.sandia.gov:8199/sfx_local?genre=article&date=2003&atitle=Streaming+dielectrophoresis+for+continuous-flow+microfluidic+devices&aulast=Cummings&auinit=EB&issn=0739-5175&volume=22&issue=6&spage=75.
- [27] A. Nakano, T.-C. Chao, F. Camacho-Alanis, A. Ros, Immunoglobulin G and bovine serum albumin streaming dielectrophoresis in a microfluidic device, *Microfluid. Miniaturization*. 32 (2011) 2314–2322.
- [28] F. Camacho-Alanis, L. Gan, A. Ros, Transitioning streaming to trapping in DC insulator-based dielectrophoresis for biomolecules, *Sensors Actuators, B Chem.* 173 (2012) 668–675. doi:10.1016/j.snb.2012.07.080.
- [29] A. Nakano, F. Camacho-Alanis, T.-C. Chao, A. Ros, Tuning direct current streaming dielectrophoresis of proteins, *Biomicrofluidics*. 6 (2012) 34108.
- [30] R. Natu, R. Martinez-Duarte, Numerical Model of Streaming DEP for Stem Cell Sorting, *Micromachines*. (2016) 217. doi:10.3390/mi7120217.
- [31] R. Martinez-Duarte, F. Camacho-Alanis, P. Renaud, A. Ros, Dielectrophoresis of lambda-DNA using 3D carbon electrodes, *Electrophoresis*. 34 (2013) 1113–1122.
- [32] M.-D.R. Islam, Monsur, Natu Rucha, Larraga-Martinez Maria Fernanda, Enrichment of diluted cell populations from large sample volumes using 3D carbon-electrode dielectrophoresis, *Biomicrofluidics*. 10 (2016).
- [33] M. Elitas, R. Martinez-Duarte, N. Dhar, J.D. McKinney, P. Renaud, Dielectrophoresis-based purification of antibiotic-treated bacterial subpopulations., *Lab Chip*. 14 (2014) 1850–7. doi:10.1039/c4lc00109e.
- [34] Y. Yildizhan, N. Erdem, M. Islam, R. Martinez-Duarte, M. Elitas, Dielectrophoretic separation of live and dead monocytes using 3D carbon-electrodes, *Sensors (Switzerland)*. 17 (2017). doi:10.3390/s17112691.
- [35] M.D.C. Jaramillo, E. Torrents, R. Martinez-Duarte, M.J. Madou, A. Juarez, On-line separation of bacterial cells by carbon-electrode dielectrophoresis, *Electrophoresis*. 31 (2010) 2921–2928.

- [36] R. Martinez-Duarte, S. Cito, E. Collado-Arredondo, S.O. Martinez, M.J. Madou, Fluid-Dynamic and Electromagnetic Characterization of 3D Carbon Dielectrophoresis with Finite Element Analysis, in: NSTI Nanotech, Boston, MA, 2008: pp. 265–268.
- [37] Z.R. Gagnon, Cellular dielectrophoresis: Applications to the characterization, manipulation, separation and patterning of cells, *Electrophoresis*. 32 (2011) 2466–2487. doi:10.1002/elps.201100060.
- [38] R. Pethig, Dielectrophoresis: Status of the theory, technology, and applications, *Biomicrofluidics*. 4 (2010) 22811. doi:10.1063/1.3456626.
- [39] C. Ming-Hsunwu, W. Chih-Yung, Y. Ruey-Hor, W. Ming-Chneg, W. An-Bang, Experimental and numerical study of the separation angle for flow around a circular cylinder at low Reynolds number, *J. Fluid Mech.* 515 (2004) 233–260.
- [40] A. Vakil, S.I. Green, Numerical Study of Two-Dimensional Circular Cylinders in Tandem at Moderate Reynolds Numbers, *J. Fluids Eng.* 135 (2013) 071204–0771213.
- [41] G. Juncu, A numerical study of momentum and forced convection heat transfer around two tandem circular cylinders at low Reynolds numbers. Part I: Momentum transfer, *Int. J. Heat Mass Transf.* 50 (2007) 3788–98.
- [42] F. Fractionation, Y. Huang, X. Wang, F.F. Becker, P.R.C. Gascoyne, Introducing Dielectrophoresis New Force Field for, 73 (1997) 1118–1129.
- [43] P.S. Williams, T. Koch, J.C. Giddings, Characterization of near-wall hydrodynamic lift forces using sedimentation field-flow fractionation, *Chem. Eng. Commun.* 111 (1992) 121–147.
- [44] J.G. Kralj, M.T.W. Lis, M.A. Schmidt, K.F. Jensen, Continuous dielectrophoretic size-based particle sorting, *Anal. Chem.* 78 (2006) 5019–5025. doi:10.1021/ac0601314.
- [45] T. Schnelle, T. Muller, G. Gradl, S.G. Shirley, G. Fuhr, Paired microelectrode system: dielectrophoretic particle sorting and force calibration, *J. Electrostat.* 47 (1999) 121–132.
- [46] M. Islam, R. Natu, R. Martinez-Duarte, Carbon MEMS for Selected Lab-on-a-Chip Applications, in: *Carbon next Silicon? Book-2 Appl.*, 2015: pp. 79–100.
- [47] R. Martinez-Duarte, R. a Gorkin, K. Abi-Samra, M.J. Madou, The integration of 3D carbon-electrode dielectrophoresis on a CD-like centrifugal microfluidic platform., *Lab Chip*. 10 (2010) 1030–43. doi:10.1039/b925456k.
- [48] J. Gilmore, M. Islam, J. Duncan, R. Natu, R. Martinez-Duarte, Assessing the importance of the root mean square (RMS) value of different waveforms to determine the strength of a dielectrophoresis trapping force, *Electrophoresis*. (2017) 1–4. doi:10.1002/elps.201600551.
- [49] R. Martinez-Duarte, Carbon-electrode Dielectrophoresis for Bioparticle Manipulation, *ECS Trans.* 61 (2014) 11–22.
- [50] M.D.C. Jaramillo, R. Martínez-Duarte, M. Hüttener, P. Renaud, E. Torrents, A. Juárez, Increasing PCR sensitivity by removal of polymerase inhibitors in environmental samples by using dielectrophoresis., *Biosens. Bioelectron.* 43 (2013) 297–303. doi:10.1016/j.bios.2012.12.049.
- [51] R. Martinez-Duarte, P. Renaud, M.J. Madou, A novel approach to dielectrophoresis using carbon electrodes, *Electrophoresis*. 32 (2011) 2385–2392.
- [52] R. Martinez-Duarte, SU-8 Photolithography as a Toolbox for Carbon MEMS, *Micromachines*. 5 (2014) 766–782.

- [53] G. Mernier, R. Martinez-Duarte, R. Lehal, F. Radtke, P. Renaud, Very High Throughput Electrical Cell Lysis and Extraction of Intracellular Compounds Using 3D Carbon Electrodes in Lab-on-a-Chip Devices, *Micromachines*. 3 (2012) 574–581.
- [54] M. Islam, R. Natu, R. Martinez-Duarte, A study on the limits and advantages of using a desktop cutter plotter to fabricate microfluidic networks, *Microfluid. Nanofluidics*. 19 (2015) 973–985. doi:10.1007/s10404-015-1626-9.
- [55] I. Ermolina, H. Morgan, The electrokinetic properties of latex particles: comparison of electrophoresis and dielectrophoresis, *J. Colloid Interface Sci.* 285 (2005) 419–428.
- [56] C.C.I. Cheng, G.Á.B.Á. Yeast, Rapid quantification of bio-particles based on image visualisation in a dielectrophoretic microfluidic chip, (2011) 311–319. doi:10.1007/s10404-010-0670-8.
- [57] O. Français, B. Le Pioufle, Lab on a Chip Micro-organism extraction from biological samples using DEP forces enhanced by osmotic shock, (2013) 901–909. doi:10.1039/c2lc41128h.
- [58] Y. Huang, R. Holzel, R. Pethig, X. Wang, Differences in the AC electrodynamic properties of viable and non-viable yeast cells determined through combined dielectrophoresis and electrorotation studies yeast cells determined through combined dielectrophoresis and, (1992).
- [59] G.H. Markx, M.S. Talary, R. Pethig, Separation of viable and non-viable yeast using dielectrophoresis, *J. Biotechnol.* 32 (1994) 29–37.
- [60] R. Martinez-Duarte, Label-free Cell Sorting using Carbon-electrode Dielectrophoresis and Centrifugal Microfluidics, University of California, Irvine, 2010.
- [61] M. Islam, J. Gilmore, K. Wallace, R. Martinez-Duarte, Dielectrophoretic characterization of *Candida* species with 3D carbon electrodes towards separation and species-specific diagnosis, in: *MicroTas*, Savannah, Georgia, 2017.
- [62] M. Henriques, Candidiasis : Predisposing Factors , Prevention , Diagnosis and Alternative Treatment, (2014) 223–240. doi:10.1007/s11046-014-9749-1.
- [63] A. Safdar, V. Chaturvedi, E.W. Cross, S. Park, E.M. Bernard, D. Armstrong, D.S. Perlin, Prospective Study of *Candida* Species in Patients at a Comprehensive Cancer Center, 45 (2001) 2129–2133. doi:10.1128/AAC.45.7.2129.
- [64] R. Singh, A. Chakrabarti, Invasive Candidiasis in the Southeast-Asian Region, in: *Candida albicans Cellular Mol. Biol.*, 2017: pp. 25–40.
- [65] N.C. Chen, C.H. Chen, M.K. Chen, L.S. Jang, M.H. Wang, Single-cell trapping and impedance measurement utilizing dielectrophoresis in a parallel-plate microfluidic device, *Sensors Actuators, B Chem.* 190 (2014) 570–577. doi:10.1016/j.snb.2013.08.104.
- [66] Y. Ai, Z. Zeng, S. Qian, Direct numerical simulation of AC dielectrophoretic particle-particle interactive motions, *J. Colloid Interface Sci.* 417 (2014) 72–79. doi:10.1016/j.jcis.2013.11.034.
- [67] M. Li, S. Li, W. Cao, W. Li, W. Wen, G. Alici, Continuous particle focusing in a waved microchannel using negative dc dielectrophoresis, *J. Micromechanics Microengineering*. 22 (2012).

Continuous Particle Separation with Streaming Dielectrophoresis

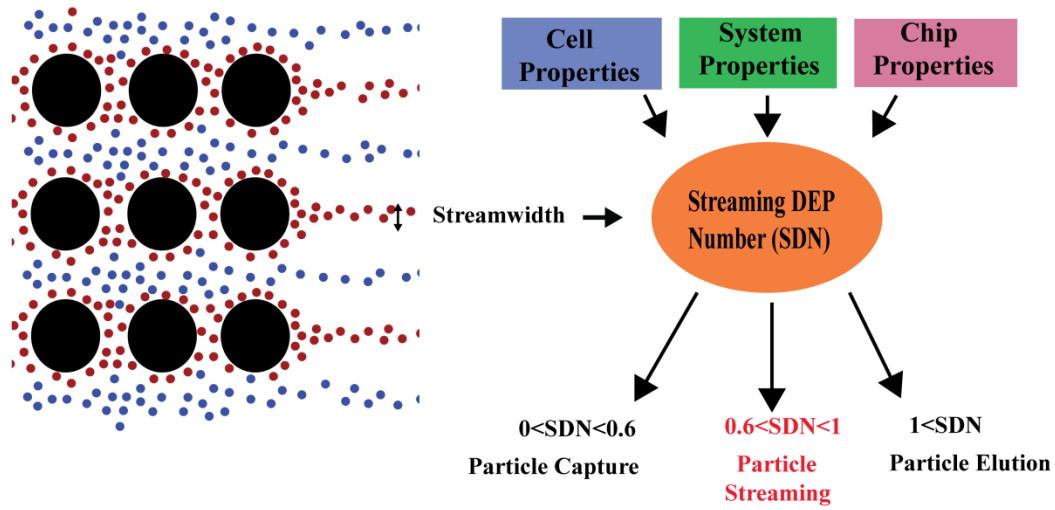


Table of Contents artwork
